QCD phase transition with Kogut-Susskind fermions on an $8^3 \times 2$ lattice

Paul F. Hsieh*
Department of Physics, Columbia University, New York, New York 10027
(Received 27 September 1990)

We report a study of the QCD finite-temperature phase transition in the presence of dynamical fermions with fermion masses ranging from 5.0 to 0.02. These calculations were performed with four flavors of Kogut-Susskind fermions on an $8^3 \times 2$ lattice using the "hybrid molecular dynamics" algorithm. The transition remains unambiguously first order for fermion masses in lattice units as low as 4.5, but weakens dramatically as the mass is reduced to 4.0. Calculations with masses of 2.0 and below show no evidence of a transition. Unlike studies with $N_t > 2$, we see no evidence of a first-order phase transition for masses as small as 0.02.

I. INTRODUCTION

Low-lying states in the hadronic spectrum illustrate two important properties of quantum chromodynamics at zero temperature: the approximate SU(2) or SU(3) chiral symmetry is spontaneously broken, and the theory confines. Both of these properties are expected to persist only for temperatures below that of the so-called QCD finite-temperature phase transition. A number of arguments including numerical calculations[1] and rigorous results for SU(2) lattice gauge theory[2] support the expectations that above some critical temperature chiral symmetry will be restored and a deconfined quark-gluon plasma will come into existence.

It has been long recognized that the finite-temperature phase transition need not persist for all values of the quark mass. The general symmetry-breaking arguments that both the pure gauge theory and the massless chiral limit possess a finite-temperature phase transition are spoiled by quarks with a finite mass; the presence or absence of such a transition becomes a complicated dynamical issue. This question has been addressed in recent years by a number of large-scale Monte Carlo calculations. Good evidence is found for a strong first-order chiral-symmetry-breaking transition when the quark mass is small, and the calculations show that the transition weakens and probably disappears as the mass is increased to intermediate values. With some exceptions,[3] current Monte Carlo evidence is consistent with, and indeed supports a picture in which the finite-temperature phase transition does not persist for all values of the quark mass.

Much of the finite-temperature fermion work has been carried out on lattices with $N_t = 4$, with spatial volumes only occasionally exceeding 8^3. Groups studying $N_t = 4$ pure gauge theory have felt the need to work on relatively large lattices; Brown *et al.*,[1] for example, have employed spatial volumes as large as 24^3, a size somewhat daunting, given the cost of dynamical fermion calculations.

The calculations reported here are an attempt to address these issues. We use Kogut-Susskind fermions for computational efficiency, and because they possess a remnant chiral symmetry at zero mass, we use four flavors because that number emerges naturally in the Kogut-Susskind formation and has received considerable attention in previous work. Our choice of $N_t = 2$, however, is less conventional. The only other $N_t = 2$ study of the nature of the finite-temperature phase transition was done for the pure gauge case and showed clear evidence for a first-order phase transition.[4] By using an $8^3 \times 2$ lattice, we gain the advantage of higher statistics on a larger volume than achievable on an $8^3 \times 4$ lattice (a $16^3 \times 4$ lattice has a naively comparable physical volume) but at a cost of working with a coarser lattice spacing that is further from the continuum, and worries about the possible breakdown of our simulation algorithm. The latter worry stems from using our algorithm with an $N_t = 2$ lattice. In the update we calculate the quantity $M^\dagger M$ where M is the Dirac matrix. In the extreme limit where all the gauge links are unitary matrices, the coupling in the time direction vanishes.

Keeping in mind our caveats about coarse lattice spacings and the $N_t = 2$ limit, we are encouraged that we can clearly resolve the pure-gauge deconfining phase transition and that the transition transforms in a sensible manner with varying quark mass. In this work we present results for a range of masses from $ma = 5.0$ to $ma = 0.02$. Going from large to intermediate fermion mass, we study how the finite-temperature transition weakens as the quark mass is reduced. At intermediate to small fermion mass, we see the transition strengthen, though we see no evidence for a reappearance of a first-order phase transition.

II. METHOD OF CALCULATION

Our current calculation was done using the hybrid-molecular-dynamics Φ algorithm of Gottlieb *et al.*[5] implemented on the 16-node lattice gauge theory computer at Columbia University.[6]

The hybrid-molecular-dynamics algorithm samples the partition function

$$Z = \int [\delta X] e^{-S(X)} \tag{1}$$

by introducing an auxiliary momentum field so that

$$Z=\int [\delta X][\delta P]e^{-[P^2/2+S(X)]} . \tag{2}$$

The hybrid algorithm periodically refreshes the momenta with a heat bath. Between heat baths, the momenta and the dynamical variables are evolved according to Hamilton's equations.

In our simulation, the action is

$$S(X)=S_G[U]+S_F[U] , \tag{3}$$

where S_G, the simple Wilson action, is given by

$$S_G[U]=\frac{\beta}{3}\mathrm{Re\,Tr}\sum_{x,\mu>\nu}(1-U^{\dagger}_{x,\nu}U_{x+\nu,\mu}U_{x+\mu,\nu}U_{x,\mu}) \tag{4}$$

and S_F, the fermionic action, is given by

$$S_F[U]=\phi^{\dagger}_e(M^{\dagger}M)^{-1}\phi_e . \tag{5}$$

$U_{x,\mu}$, the gauge field, resides as SU(3) matrices on each link of the lattice. ϕ_e, the Kogut-Susskind fermion field, resides on even sites of the lattice. $\beta=6/g^2$, where g is the gauge coupling. M, for Kogut-Susskind fermions, is defined as

$$M[U]_{i,j}=m\delta_{ij}+\tfrac{1}{2}\sum_{\mu}\sigma_{i,\mu}(U^{\dagger}_{i,\mu}\delta_{i,j-\mu}-U_{i-\mu,\mu}\delta_{i,j+\mu}), \tag{6}$$

where m is the quark mass and $\sigma_{i,\mu}$ are the Kogut-Susskind sign factors.

The fermionic fields and the momenta are refreshed with a heat bath at the beginning of each trajectory. During the molecular dynamics evolution, the fermionic fields are kept fixed.

In the heat bath we set

$$\phi=M^{\dagger}\eta , \tag{7}$$

$$P_{i,\mu}=\frac{1}{\sqrt{2}}\sum\lambda_a\eta , \tag{8}$$

where λ_a are the eight Gell-Mann matrices normalized as $\mathrm{Tr}(\lambda_a\lambda_b)=2\delta_{ab}$, η is a normal deviate, and $\boldsymbol{\eta}$ is a complex vector of normal deviates.

Hamilton's equations for our system take the form

$$\dot{U}_{i\mu}=iP_{i\mu}U_{i\mu} \tag{9}$$

and, for even sites,

$$i\dot{P}_{i,\mu}=-\frac{\beta}{3}(U_{i,\mu}\{V_{i,\mu}-\sigma_{i,\mu}[(M^{\dagger}M)^{-1}\phi]_i\otimes[(M^{\dagger})^{-1}\phi^*]_{i+\mu}\})_{\mathrm{TA}} \tag{10}$$

and, for odd sites,

$$i\dot{P}_{i,\mu}=-\frac{\beta}{3}(U_{i,\mu}\{V_{i,\mu}+\sigma_{i,\mu}[(M^{\dagger})^{-1}\phi]_i\otimes[(M^{\dagger}M)^{-1}\phi^*]_{i+\mu}\})_{\mathrm{TA}} . \tag{11}$$

$V_{i,\mu}$ is the sum of the six staples that surround the link $U_{i,\mu}$, "TA" means to take the traceless anti-Hermitian part, and $\otimes$ is the exterior product defined as

$$(\phi\otimes\psi)_{ab}\equiv\phi_a\cdot\psi_b . \tag{12}$$

We numerically integrate these equations using the "leapfrog" method:

$$P(\tau_0+\tfrac{1}{2}\Delta\tau)=P(\tau_0)+\tfrac{1}{2}\Delta\tau\dot{P}(\tau_0) , \tag{13}$$

$$U(\tau_n+\Delta\tau)=\exp[i\Delta\tau P(\tau_n+\tfrac{1}{2}\Delta\tau)]U(\tau_n) , \tag{14}$$

$$P(\tau_n+\tfrac{1}{2}\Delta\tau)=P(\tau_{n-1}+\tfrac{1}{2}\Delta\tau)+\Delta\tau\dot{P}(\tau_n) , \tag{15}$$

where $\tau_n=\tau_0+n\Delta\tau$.

We run using a step size of $\Delta\tau=0.02$ and 0.025. Each step requires an exponentiation and an inversion of the fermionic determinant. We use a fourth-order Taylor polynomial for the exponentiation and we reunitarize the resulting matrix. We use a conjugate gradient to invert the fermionic determinant. We stop with a typical residual squared of 5×10^{-5} across the lattice. For masses of $ma=0.05$ and 0.02 we relaxed this condition to 5×10^{-3}. We thermalize the system every 0.5 units of time. For our heat bath we generate normal deviates using Forsythe's method and uniform deviates using a Fibonacci generator with a period exceeding 2^{55}.[7]

The following observables were measured every five $\Delta\tau$ units of time: the Polyakov loop

$$\mathcal{P}=\tfrac{1}{3}\mathrm{tr}\left[\prod_t U_{(t,\mathbf{x})}\right] \tag{16}$$

and the plaquette action

$$\square=1-\tfrac{1}{3}\mathrm{Re\,Tr}(U^{\dagger}_{x,\nu}U_{x+\nu,\mu}U_{x+\mu,\nu}U_{x,\mu})_{\mathbf{x},\mu>\nu} . \tag{17}$$

The chiral condensate

$$\bar{\psi}\psi=\tfrac{1}{3}\mathrm{tr}(M^{-1})=\boldsymbol{\eta}^*M^{-1}\boldsymbol{\eta} , \tag{18}$$

where $\boldsymbol{\eta}$ is a complex vector of Gaussian noise $\langle\boldsymbol{\eta}^*\boldsymbol{\eta}\rangle=1$, was measured every 0.5 units of time.

The 16-node Columbia machine only does floating-point arithmetic to 22-bits precision. Empirically, we have found this degree of precision sufficient for the current calculation. The most direct check of the correctness of our implementation has been made by the newest Columbia machine which has 32-bit precision.[8] An independent implementation of an exact hybrid Monte Carlo algorithm[9] reproduced some results done by our current calculation at $m=2.0$ and $m=0.02$. This gives us a fair degree of confidence in our current program in both the high- and low-mass regimes.

As a check of our simulation parameters, we did two simulations at $m=4.25$. With a step size of $\Delta t=0.02$, and 50 conjugate-gradient iterations we see a bimodal signal at $\beta=5.040$ (Figs. 6 and 12). With $\Delta t=0.01$, and 100 conjugate-gradient iterations, the configuration was much more deconfined than our original simulation. Lowering

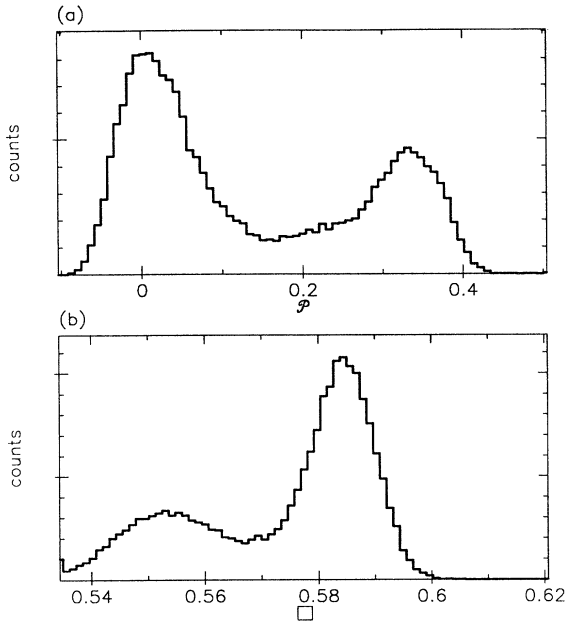

FIG. 1. Data from an $8^3\times 2$ heat-bath simulation. Histograms of (a) the real part of the "wrapped" Polyakov loop and (b) the elementary plaquette at the critical coupling $\beta=5.090$. Clear two-peaked structure is seen. "Wrapping" the Polyakov loop $\mathcal{P}=|P|e^{i\theta}\rightarrow|P|e^{i3\theta}=\mathcal{P}_{\text{wrapped}}$ allows for comparison of pure gauge measurements with finite-mass measurements.

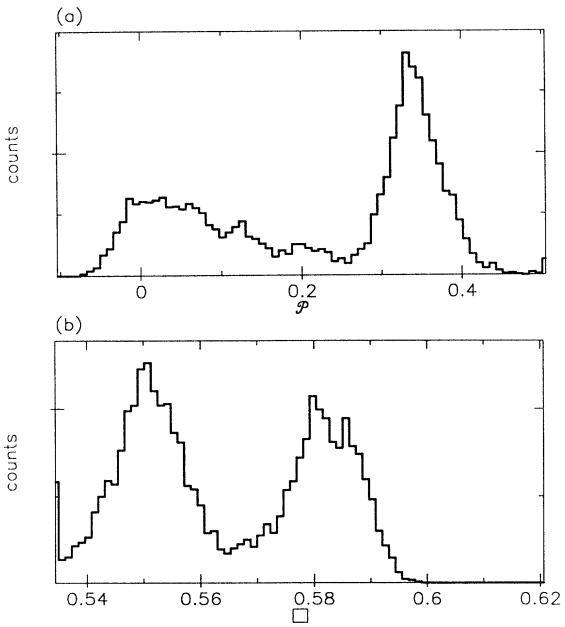

FIG. 2. Data from $m=\infty$, $\beta=5.092$ simulation. Histograms of (a) the real part of the Polyakov loop and (b) the elementary plaquette. These histograms are made from a cold start and reproduce the results from Fig. 1.

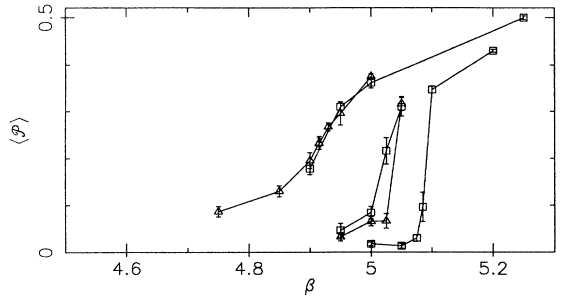

FIG. 3. Curves used to find critical points. Included are $m=2.0$, 4.0, and ∞. From $m=2.0$ and 4.0, averages of the real part of the Polyakov loop from times $t=200$–400 of both hot and cold starts are plotted. Measurements for $m=\infty$ are from a heat-bath simulation and included only for comparison. Lines are included to help guide the eye.

to $\beta=5.035$ we managed to produce a simulation quite similar to our original run (Fig. 17). This "shift" in β we attribute to finite-step-size effects, but we emphasize that we have reproduced the qualitative features of the phase transition from our earlier run.

We spend 10% of our calculation checking for hardware errors. The 16-node machine is configured as a 4×4 torus with each node containing a $2\times 2\times 8\times 2$ sublattice. Roughly every half hour, the lattice configuration is "translated" one node and the previous three minutes worth of calculation is duplicated and compared. After six months of running, we have yet to detect a hardware error with this test.

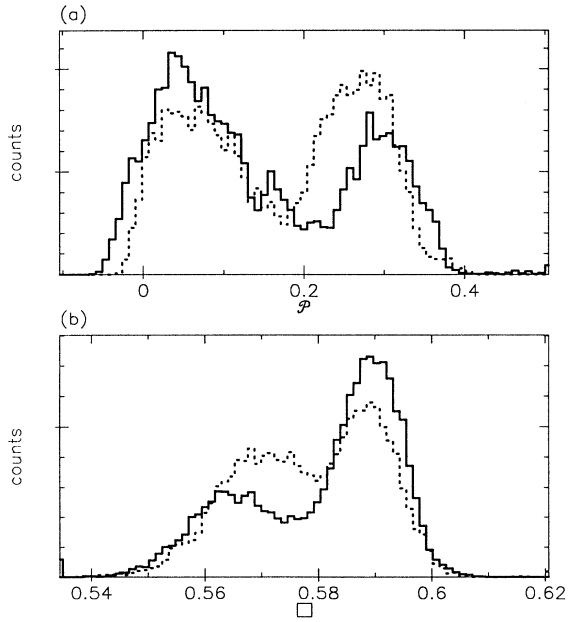

FIG. 4. Data from $m=5.00$, $\beta=5.05$ simulation. Histograms of (a) the real part of the Polyakov loop and (b) the elementary plaquette. Dotted lines correspond to hot start, solid lines correspond to cold start.

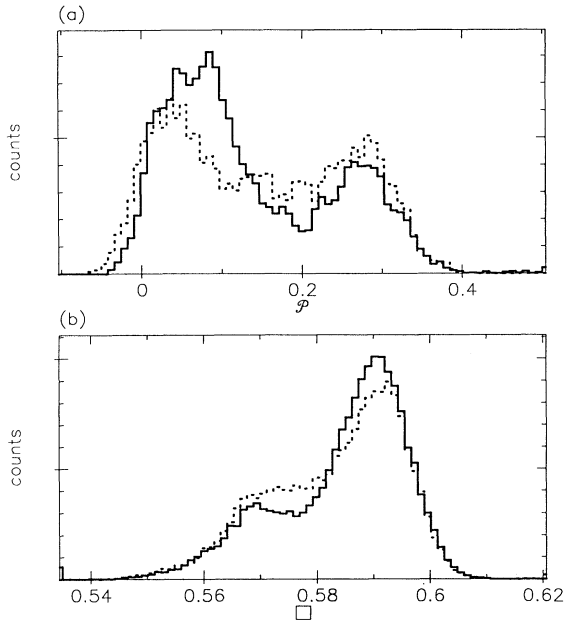

FIG. 5. Data from $M=4.50$, $\beta=5.037$ simulation. Histograms of (a) the real part of the Polyakov loop and (b) the elementary plaquette. Dotted lines correspond to hot start, solid lines correspond to cold start.

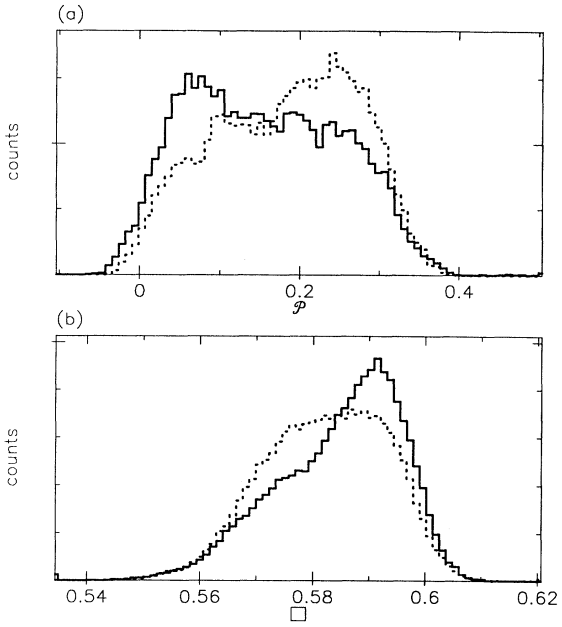

FIG. 7. Data from $m=4.00$, $\beta=5.025$ simulation. Histograms of (a) the real part of the Polyakov loop and (b) the elementary plaquette. Dotted lines correspond to hot start, solid lines correspond to cold start. Two-peaked structure is much less apparent than $m=4.25$ case.

III. SIGNAL FOR A FIRST-ORDER PHASE TRANSITION

First-order phase transitions are characterized by discontinuities in the first derivatives in the free energy of the system. In the case of lattice QCD, we look for discontinuities in the Polyakov $\mathcal{P}$ and the chiral condensate $\bar{\psi}\psi$ order parameters as a function of temperature.

For systems with a first-order phase transition we say

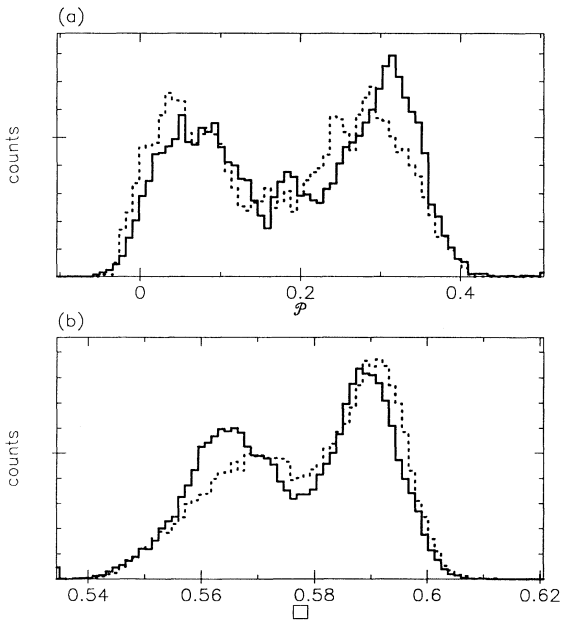

FIG. 6. Data from $m=4.25$, $\beta=5.040$ simulation. Histograms of (a) the real part of the Polyakov loop and (b) the elementary plaquette. Dotted lines correspond to hot start, solid lines correspond to cold start.

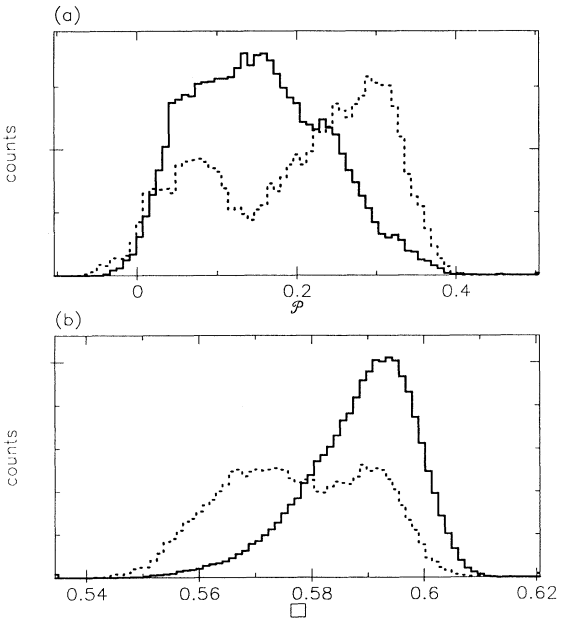

FIG. 8. Data from $m=3.50$, $\beta=5.006$ simulation. Histograms of (a) the real part of the Polyakov loop and (b) the elementary plaquette. Dotted lines correspond to hot start, solid lines correspond to cold start.

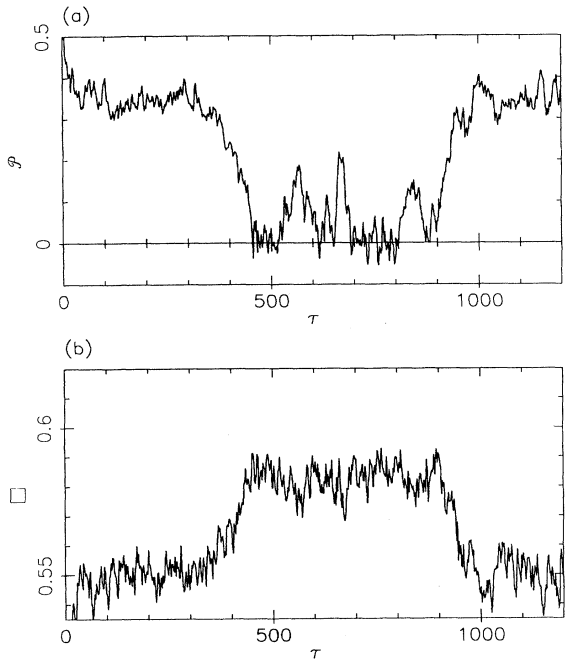

FIG. 9. Data from $m=\infty$, $\beta=5.092$ simulation. Run history of (a) the real part of the Polyakov loop and (b) the elementary plaquette. This run is from a cold start.

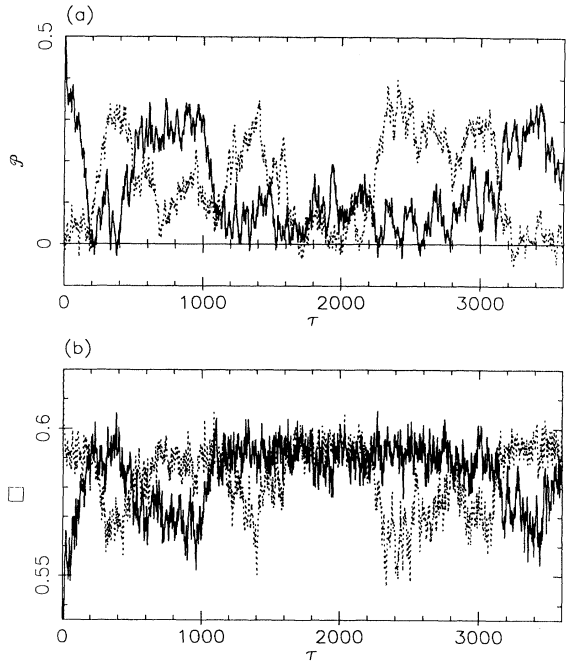

FIG. 11. Data from $m=4.50$, $\beta=5.037$ simulation. Run history of (a) the real part of the Polyakov loop and (b) the elementary plaquette. Solid lines are cold start, dotted lines are hot start.

that the system exhibits two phases, a low-temperature phase and a high-temperature phase, separated by the phase transition. At the point of discontinuity, the critical point, the system admits the existence of both the

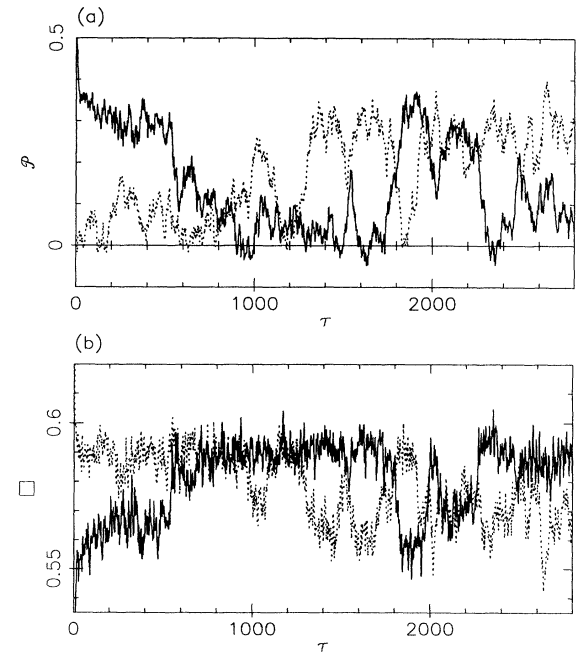

FIG. 10. Data from $m=5.00$, $\beta=5.05$ simulation. Run history of (a) the real part of the Polyakov loop and (b) the elementary plaquette. Solid lines are cold start, dotted lines are hot start.

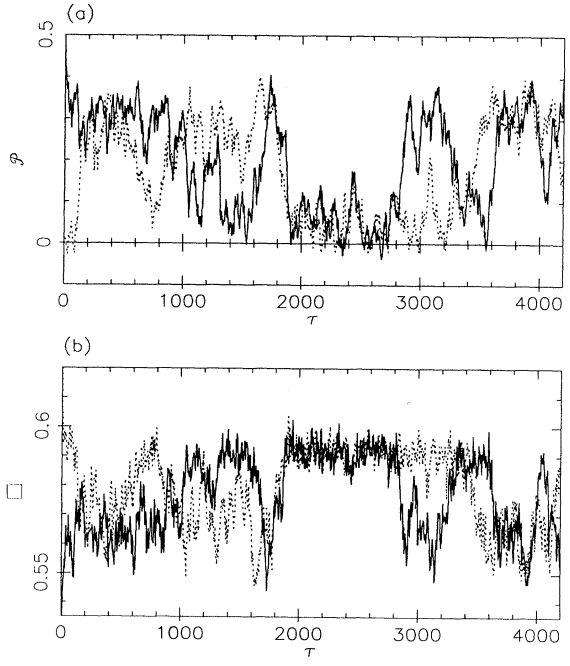

FIG. 12. Data from $m=4.25$, $\beta=5.040$ simulation. Run history of (a) the real part of the Polyakov loop and (b) the elementary plaquette. Solid lines are cold start, dotted lines are hot start.

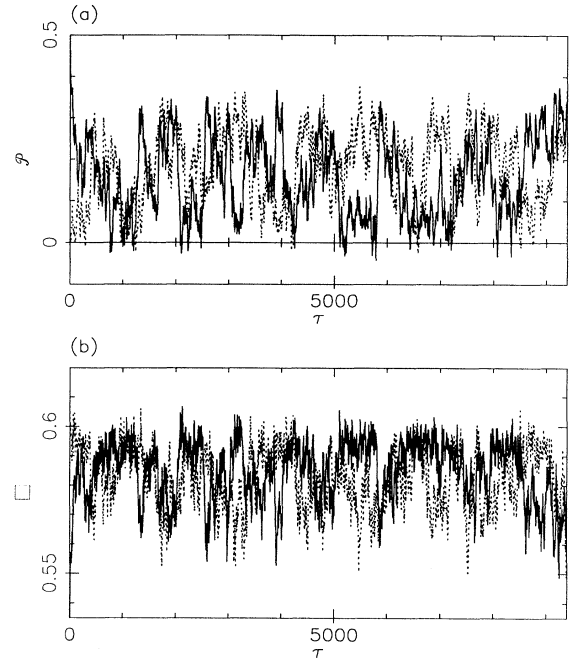

FIG. 13. Data from $m=4.00$, $\beta=5.025$ simulation. Run history of (a) the real part of the Polyakov loop and (b) the elementary plaquette. Solid lines are cold start, dotted lines are hot start.

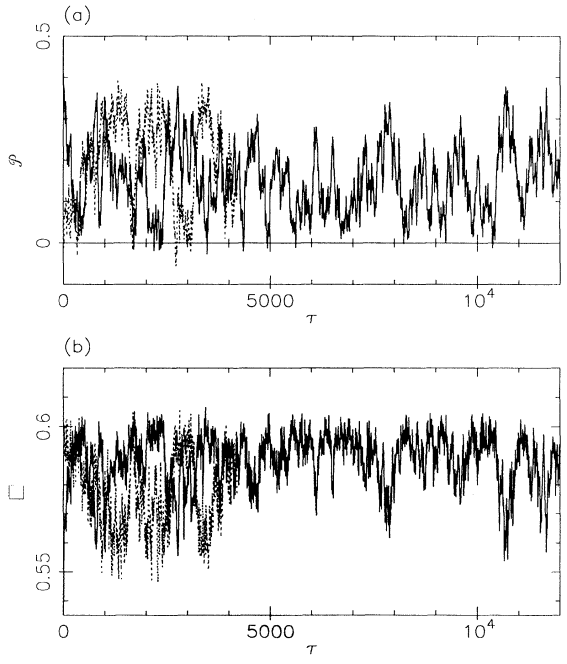

FIG. 14. Data from $m=3.50$, $\beta=5.006$ simulation. Run history of (a) the real part of the Polyakov loop and (b) the elementary plaquette. Solid lines are cold start, dotted lines are hot start.

low-temperature phase and the high-temperature phase.

In finite models of systems with first-order phase transitions, true discontinuities do not develop. In taking a statistical average over enough configurations, the order parameters will converge to unique values for all temperature, even the critical temperature. The reason for this is that near the critical temperature, the two phases become metastable and the system will tunnel between the high-temperature phase and the low-temperature phases. This coexistence of two metastable phases in a finite-sized model is a clear signal for the presence of a first-order phase transition in our system.

In our computer simulation we sample $\mathcal{P}$ and $\bar{\psi}\psi$ at regular intervals, generally every tenth of a unit of microcanonical time. For points away from the critical point we expect thermodynamic fluctuations to cause our measurements to obey a Gaussian probability distribution centered at the expectation value of our observables. The signal for a first-order phase transition is a probability distribution that corresponds to a double Gaussian with an interfacial correction.[10]

Since our goal is to classify various masses in terms of whether they exhibit a first-order phase transition or not, it is not necessary to accurately determine the relative heights and widths of the double Gaussian peaks at the critical point. We are content to see a clear two-peaked structure in the histogram of $\bar{\psi}\psi$ or $\mathcal{P}$.

We search for the critical point by making several runs over the region in temperature where the system crosses between the presumed low-temperature phase and the presumed high-temperature phase. For each temperature, we make runs from both an ordered (gauge fields set to unity) lattice or a disordered [random SU(3) gauge fields] lattice. This serves the dual purpose of probing for metastable behavior near the critical point, and giving a handle on equilibrium time when we are far from the critical point.

Unfortunately, there is no correspondingly definitive signal that indicates the absence of a first-order phase transition in a system. Instead, what we look for is a smooth continuous crossover between low-temperature and high-temperature regimes. In lattice QCD simulations, this can be rather treacherous because of the long equilibration time of the system. Early investigations were misled by what was thought to be hysteresis (and therefore a signal for first-order phase transition) when, in fact, what was seen was the result of slow equilibration.

In our studies, by taking disordered and ordered starts for each temperature, we are able to get an unbiased measurement of $\mathcal{P}$ and $\bar{\psi}\psi$ in the transition region. When the hot start measurements and the cold start measurements converge together for all values of β giving us a smooth crossover between the high- and low-temperature regimes, we say the system does not have a first-order phase transition.

IV. RESULTS

We have performed a series of calculations with four-flavor Kogut-Susskind fermions on an $8^3\times 2$ lattice. At large mass values, we have studied masses of $ma=5.00$,

4.50, 4.25, 4.00, 3.50, 3.00, and 2.00 as well as the pure gauge case of $ma = \infty$. For this range in masses, we present histograms and evolutions for the Polyakov loop and elementary plaquette that show the structure of the deconfining phase transition as it weakens with decreasing mass. At intermediate to small mass, we present results from simulation with $ma = 1.2$, 1.0, 0.8, 0.5, 0.1, 0.05, and 0.02. For these small values, examination of the Polyakov loop and chiral condensate shows continued broadening followed by a gradual sharpening of the crossover region. However, no reappearance of a first-order transition is observed.

A. Pure gauge result

In light of our comments in Sec. I about the weakness of the pure gauge transition, let us begin with a comparison of pure gauge calculations performed with the same hybrid-molecular-dynamics program used for the finite-mass calculations, and with a conventional heat-bath program.[11] Figures 1 and 2 show the histograms of the measurements from the heat bath and the hybrid program (see Fig. 9 for corresponding evolutions).

First, note that these runs are a good test of the correctness of the molecular dynamics program: the correct physical structure of the transition is obtained. Next, we emphasize that the first-order deconfinement transition is clearly resolved; the Polyakov loop histogram shows a clear two-phase structure, which is seen again more weakly in the bimodal plaquette histogram. These pure gauge calculations show that only a finite-

TABLE I. The long runs at β_{critical} that were made in order to observe bimodal behavior. Note that for $ma = 4.00$ and $ma = 3.50$ no clear signal could be observed even with 20 000 units of time.

ma	β	Run length	Comment
5.00	5.050	5600	Clear bimodal signal Figs. 4 and 10
4.50	5.037	7200	Clear bimodal signal Figs. 5 and 11
4.25	5.040	8400	Clear bimodal signal Figs. 6 and 12
4.00	5.025	19 000	Large fluctuations No clear bimodal signal Figs. 7 and 13
3.50	5.006	24 000	Large fluctuations No clear bimodal signal Figs. 8 and 14
3.00	5.000	8000	Large fluctuations No clear bimodal signal
2.00	4.750	400	Smaller fluctuations
	4.850	400	Transition region becoming
	4.900	5600	smooth
	4.915	4800	
	4.930	2400	
	4.950	800	
	5.000	800	
	5.250	400	

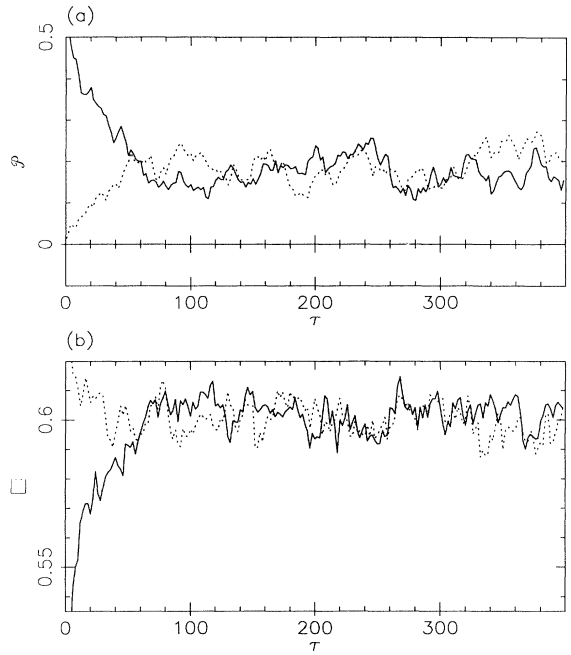

FIG. 15. Data from $m = 2.0$, $\beta = 4.90$ that show very continuous behavior. Run history of (a) the real part of the Polyakov loop and (b) the elementary plaquette. Solid lines are cold start, dotted lines are hot start.

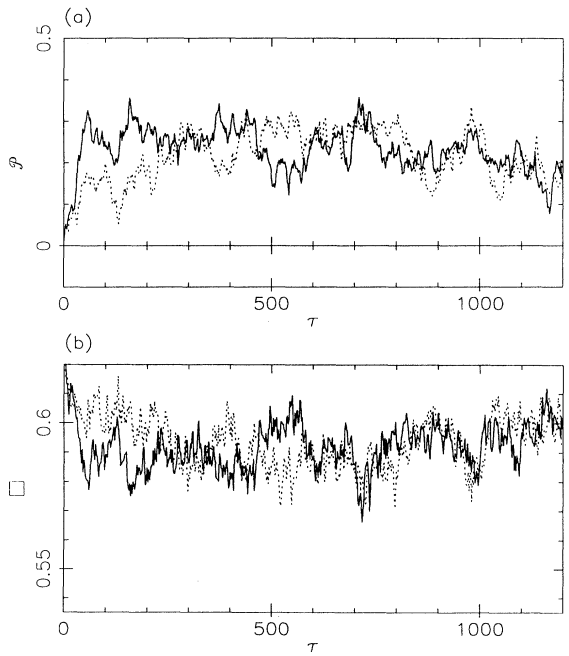

FIG. 16. Data from $m = 2.0$, $\beta = 4.915$ that show very continuous behavior. Run history of (a) the real part of the Polyakov loop and (b) the elementary plaquette. Both runs are from hot starts.

temperature transition significantly weaker than pure gauge deconfinement could have been missed by the 8^3 volume and statistics of the dynamical fermion calculations presented here.

B. High masses

In order to locate the critical point, we look for signs of metastability in the critical region. To this end, we do hot and cold starts for 400 units of time and we examine the last 200 units of time. In Fig. 3 we show this for masses of $ma=4.00$ and $ma=2.00$. We see that there is a rather noticeable gap for $ma=4.00$. For $ma=2.00$ this crossover region is very smooth; hot and cold starts converge rapidly to a stable value. To show how much this crossover-transition region has broadened, we have also included pure gauge results in Fig. 3.

Histograms of the Polyakov loop and plaquette are shown in Figs. 4–8 for a series of masses decreasing from 5.0 to 3.5, with corresponding evolutions given in Figs. 10–14. These runs are the basis for our principal result and are summarized in Table I. The strength of the transition, as given, for example, by the separation of the peaks in the Polyakov loop histograms, decreases modestly as the mass is decreased from 5.00 to 4.25, but then more sharply as the mass is decreased to 4.00. In fact, at masses of 4.0 and 3.5, even with runs of 20 000 units of microcanonical time, no clean bimodal signal is seen in the histograms, although they do show significant structure. The simplest interpretation of the data at these masses is that the first-order transition persists down to $m=3.5$, but has become rather weak by $m=4.0$, and shows finite-volume smearing. Possible alternatives such as a second-order transition, or a sharp, but continuous crossover, are most easily probed by with larger volumes.

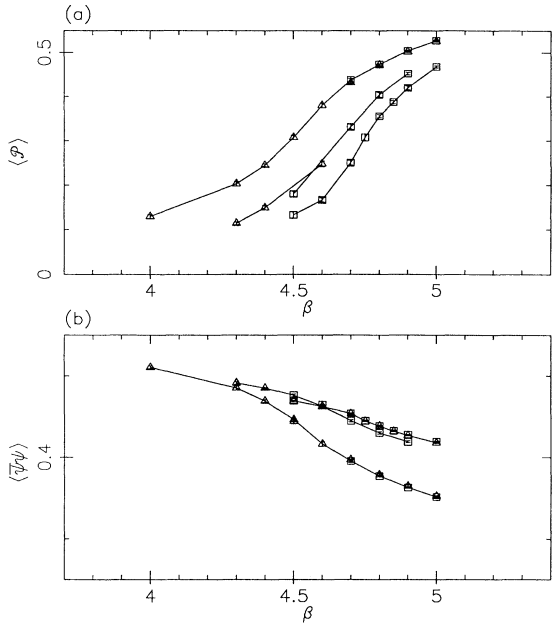

FIG. 18. Transition region measurements for several masses (0.5, 0.8, 1.0). (a) is the real part of the Polyakov loop and (b) is the chiral condensate. Triangles represent hot starts and boxes represent cold starts.

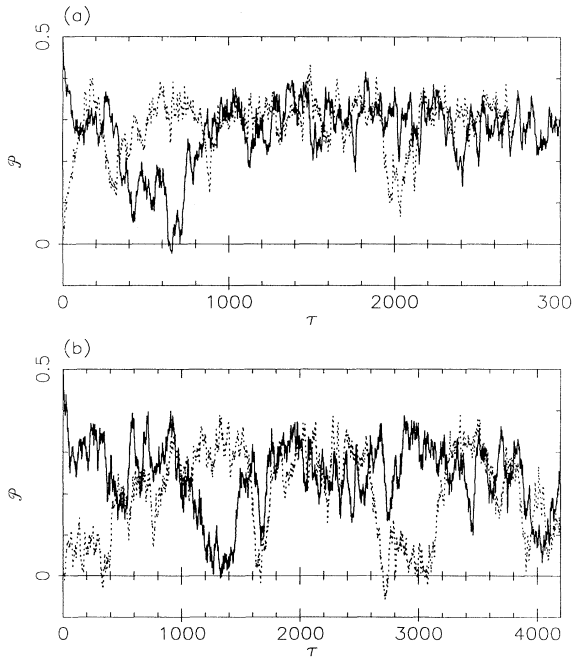

FIG. 17. Run history and histogram of a $m=4.25$ run with step size of 0.01 and 100 conjugate-gradient sweeps. (a) shows the results for $\beta=5.040$ which is apparently deconfined. (b) shows a two-state signal at $\beta=5.035$. Solid lines are cold start, dotted lines are hot start.

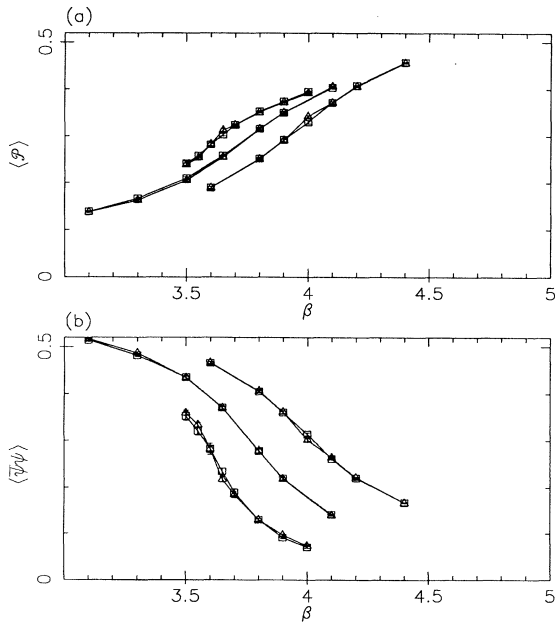

FIG. 19. Transition region measurements for several masses (0.02, 0,05, 0.1). (a) is the real part of the Polyakov loop and (b) is the chiral condensate. Triangles represent hot starts and boxes represent cold starts. Notice the progressive sharpening of the chiral condensate as mass is decreased.

TABLE II. Values for the chiral condensate and the Polyakov loop at fermion mass, (a) $ma=1.20$, (b) $ma=1.00$, (c) $ma=0.80$, (d) $ma=0.50$, (e) $ma=0.10$, (f) $ma=0.05$, on an $8^3\times2$ lattice. The run length is given in units of microcanonical time and indicates the number of units of time that was discarded to allow for equilibration.

ma	N_s	β	Start	$\langle\bar{\psi},\psi\rangle$	$\langle\mathcal{P}\rangle$	Run length
			(a)			
1.20	8	4.30	Hot	0.459(1)	0.077(3)	400–200
		4.60	Hot	0.452(2)	0.128(5)	400–200
		4.70	Hot	0.444(1)	0.189(5)	400–200
		4.75	Cold	0.439(1)	0.242(14)	400–200
			Hot	0.440(2)	0.236(7)	400–200
		4.80	Cold	0.431(1)	0.310(13)	400–200
		4.90	Cold	0.423(1)	0.382(7)	400–200
		5.00	Cold	0.415(1)	0.444(5)	400–200
		5.10	Cold	0.409(1)	0.489(2)	400–200
			Cold	0.409(1)	0.489(2)	400–200
			(b)			
1.00	8	4.50	Cold	0.470(1)	0.133(7)	750–200
			Hot	0.469(1)	0.131(6)	750–200
		4.60	Cold	0.465(1)	0.167(5)	750–200
			Hot	0.463(1)	0.179(6)	750–200
		4.70	Cold	0.454(1)	0.250(5)	750–200
			Hot	0.454(1)	0.240(7)	750–200
		4.75	Cold	0.445(1)	0.307(8)	750–200
			Hot	0.445(1)	0.310(7)	750–200
		4.80	Cold	0.439(1)	0.355(4)	750–200
			Hot	0.439(1)	0.347(7)	750–200
		4.85	Cold	0.433(1)	0.387(4)	750–200
			Hot	0.432(1)	0.391(7)	750–200
		4.90	Cold	0.428(1)	0.420(5)	750–200
			Hot	0.427(1)	0.421(3)	750–200
		5.00	Cold	0.419(1)	0.468(2)	750–200
			Hot	0.418(1)	0.469(2)	750–200
			(c)			
0.80	8	4.30	Hot	0.491(2)	0.114(4)	400–200
		4.40	Hot	0.485(1)	0.149(5)	400–200
		4.50	Cold	0.476(2)	0.180(6)	400–200
		4.60	Hot	0.463(2)	0.247(7)	400–200
		4.70	Cold	0.445(2)	0.331(6)	400–200
		4.80	Cold	0.430(1)	0.404(5)	400–200
		4.90	Cold	0.419(1)	0.452(3)	400–200
			(d)			
0.50	8	4.00	Hot	0.511(2)	0.130(5)	200–100
		4.30	4.00	0.481(2)	0.212(12)	200–100
			4.40	0.485(3)	0.203(6)	200–100
		4.40	4.50	0.469(2)	0.244(3)	200–100
		4.50	Hot	0.447(2)	0.307(5)	800–200
			4.60	0.444(3)	0.307(6)	200–100
		4.60	4.70	0.417(3)	0.380(6)	200–100
		4.70	Cold	0.395(2)	0.437(5)	400–200
			Hot	0.397(1)	0.431(3)	400–200
		4.80	Cold	0.377(1)	0.473(2)	400–200
			Hot	0.379(1)	0.472(3)	400–200
		4.90	Cold	0.363(1)	0.504(2)	400–200
			Hot	0.365(1)	0.502(2)	400–200
		5.00	Cold	0.351(1)	0.527(2)	400–200
			Hot	0.353(1)	0.526(2)	400–200

TABLE II. (*Continued*).

ma	N_s	β	Start	$\langle\bar{\psi},\psi\rangle$	$\langle\mathcal{P}\rangle$	Run length
			(e)			
0.10	8	3.60	Cold	0.465(2)	0.190(2)	750–200
			Hot	0.466(2)	0.189(2)	750–200
		3.80	Cold	0.405(2)	0.252(2)	750–200
			Hot	0.406(3)	0.251(3)	750–200
		3.90	Cold	0.360(3)	0.292(3)	750–200
			Hot	0.361(3)	0.291(3)	750–200
		4.00	Cold	0.314(3)	0.330(4)	750–200
			Hot	0.302(3)	0.342(2)	750–200
		4.10	Cold	0.262(2)	0.371(2)	750–200
			Hot	0.264(2)	0.371(2)	750–200
		4.20	Cold	0.220(2)	0.407(1)	750–200
			Hot	0.221(1)	0.405(1)	750–200
		4.40	Cold	0.167(1)	0.457(1)	750–200
			Hot	0.167(1)	0.456(1)	750–200
			(f)			
0.05	8	3.10	Cold	0.514(3)	0.139(2)	750–200
			Hot	0.516(2)	0.138(1)	750–200
		3.30	Cold	0.482(3)	0.167(2)	750–200
			Hot	0.487(2)	0.163(2)	750–200
		3.50	Cold	0.435(4)	0.210(3)	750–200
			Hot	0.434(3)	0.205(2)	750–200
		3.65	Cold	0.370(3)	0.258(2)	750–200
			Hot	0.370(4)	0.255(4)	750–200
		3.80	Cold	0.278(4)	0.316(3)	750–200
			Hot	0.279(4)	0.315(3)	750–200
		3.90	Cold	0.220(4)	0.350(3)	750–200
			Hot	0.218(3)	0.350(2)	750–200
		4.10	Cold	0.141(2)	0.403(1)	750–200
			Hot	0.139(1)	0.405(2)	750–200

TABLE III. Values for the chiral condensate and the Polyakov loop at fermion mass $ma=0.02$ on an $N_s^3\times 2$ lattice. The run length is given in units of microcanonical time and indicates the number of units of time that was discarded to allow for equilibration. Note that the corresponding measurements for $N_s=8$ and 16 are identical.

ma	N_s	β	Start	$\langle\bar{\psi}\psi\rangle$	$\langle\mathcal{P}\rangle$	Run length
0.02	8	3.50	Cold	0.353(9)	0.242(5)	600–200
			Hot	0.359(6)	0.239(3)	600–200
		3.55	Cold	0.321(8)	0.258(4)	600–200
			Hot	0.334(5)	0.253(4)	600–200
		3.60	Cold	0.283(5)	0.282(3)	600–200
			Hot	0.283(12)	0.283(7)	600–200
		3.65	Cold	0.235(6)	0.303(3)	600–200
			Hot	0.217(6)	0.313(4)	600–200
		3.70	Cold	0.189(8)	0.324(2)	600–200
			Hot	0.184(6)	0.324(2)	600–200
		3.80	Cold	0.130(3)	0.352(2)	600–200
			Hot	0.130(3)	0.351(2)	600–200
		3.90	Cold	0.091(2)	0.374(2)	600–200
			Hot	0.096(2)	0.372(1)	600–200
		4.00	Cold	0.071(2)	0.395(1)	600–200
			Hot	0.074(1)	0.391(1)	600–200
	16	3.65	Cold	0.231(2)	0.301(2)	400–200
			Hot	0.227(6)	0.302(3)	400–200
		3.70	Cold	0.192(2)	0.319(1)	400–200
			Hot	0.189(3)	0.321(2)	400–200

Finally at a mass of 2.0, we see no evidence for a transition. The $m=2.0$ runs shown in Figs. 15 and 16 were performed for β in the region of sharpest β dependence. These runs are supportive of, and fully consistent with, the absence of a phase transition at this mass.

C. Intermediate and low mass

In our attempt to locate a critical region for lower masses, again we look for signs of metastability. Starting from hot and cold starts, we do simulations of 600–700 units of time, throwing away the first 200 units of time to allow for thermalization. Figures 18 and 19, and Tables II and III, represent measurements of the Polyakov loop and the chiral condensate obtained for masses between 1.0 and 0.02. As you can see, all of these are very smooth with no discernible gap.

We observe in Figs. 18 and 19 that the chiral condensate begins to show some structure in the crossover region at masses below 0.5. The transition region continues to sharpen as the mass is decreased to 0.02, but no discontinuity develops.

To further examine the $m=0.02$ case, we have made runs using the 256-node Columbia machine on a $16^3\times 2$ lattice at $\beta=3.65$ and $\beta=3.7$. We see from Table III that even with greater precision, larger volumes, and using an exact algorithm, the results show a smooth transition region with no discernible gap.

The failure to find the appearance of a first-order chiral phase transition is rather surprising. First-order chiral phase transitions have been found for $ma=0.01$ on lattices with $N_t=8$ (Ref. 12) and on $N_t=4$, and $N_t=6$ lattices using the same 256-node machine and program that fails to find a first-order transition for $N_t=2$.[13] It is believed that for $N_t=4$, the first-order transition persists to $ma=0.15$.[13] Naively, one would expect to see first-order behavior on an $N_t=2$ lattice at a mass as high as $ma=0.1$.

V. CONCLUSIONS

We have used an $8^3\times 2$ lattice to study the qualitative features of the QCD finite-temperature phase transition as a function of fermion mass. For high masses, we see evidence for a first-order phase transition that results from deconfinement. As we lower the fermion mass from 5.00 to 2.00, we see the disappearance of this phase transition. Below a mass of 4.00, we see fluctuations increase and the two-peak structure wash out. These effects are consistent with a phase boundary disappearing at a second-order critical point. For intermediate and low masses, the behavior is characterized by a smooth crossover between high- and low-temperature regimes for masses as low as 0.02.

Our direct measurement of the disappearance of the deconfining phase transition at intermediate mass is consistent with, and serves to confirm, the failure of earlier $N_t=4$ calculations to find a first-order phase transition in the mass region between $ma=0.2$ and $ma=1.00$. But as we have noted in the previous section, our failure to see a low-mass first-order phase transition is surprising. In four-flavor simulations, a first-order chiral phase transition has been observed at $ma=0.05$ on a $16^3\times 4$ lattice, at $ma=0.01$ on a $16^3\times 6$ lattice,[13] and at $ma=0.01$ on a $16^3\times 8$ lattice.[12] At the critical point, $ma=0.02$ on an $8^3\times 2$ lattice would naively correspond to $ma=0.01$ on a $16^3\times 4$ lattice, $ma=0.007$ on a $24^3\times 6$ lattice, and $ma=0.005$ on a $32^3\times 8$ lattice. On the $8^3\times 2$ lattice we see none of the clear metastability seen on the $16^3\times 4$, 6, and 8 lattices. We do, however, see a progressive sharpening of our Polyakov loop and chiral condensate observables. At this point it seems possible that no first-order transition will appear for small fermion mass on $8^3\times 2$ lattices.

Lattices with $N_t=2$ appear to be anomalous in their failure to exhibit a strong chiral phase transition at low quark mass. This anomalous behavior is not well understood and worries about the behavior of the update procedure on $N_2=2$ lattices mentioned in Sec. I only further confuse the issue. Future studies of $N_t=2$ lattices may be advised to use alternative update procedures to minimize these worries. The high-mass behavior, however, seems consistent with lattices with larger temporal extent. We believe these measurements present a good qualitative picture of the disappearance of the deconfining phase transition in lattice QCD.

ACKNOWLEDGMENTS

The author thanks F. R. Brown and N. H. Christ for many helpful discussions during the work of this paper. The calculations were performed on the Columbia University 16-node QCD machine which was built by N. H. Christ and H.-Q. Ding. This work was supported in part by the U.S. Department of Energy.

*Present address: Department of Physics, Brookhaven National Laboratory, Upton, NY 11973.

[1]The following are two recent publications on numerical studies of pure-gauge deconfinement transitions. References to earlier works can be found in these: F. R. Brown *et al.*, Phys. Rev. Lett. **61**, 2058 (1988); M. Fukugita *et al.*, Nucl. Phys. **B337**, 181 (1990).

[2]E. Tomboulis and L. Yaffe, Phys. Rev. D **29**, 780 (1984).

[3]R. Gupta, G. Kilcup, and S. Sharpe, Phys. Rev. D **38**, 1288 (1988).

[4]A. D. Kennedy *et al.*, Phys. Rev. Lett. **54**, 87 (1985).

[5]S. Gottlieb, W. Liu, D. Toussaint, R. Renken, and R. Sugar, Phys. Rev. D **35**, 2531 (1987).

[6]N. H. Christ and A. E. Terrano, IEEE Trans. Comput. **33**, 344 (1984); Byte Magazine **11** (4), 145 (1986).

[7]D. E. Knuth, *Seminumerical Algorithms,* 2nd ed. (Addison-Wesley, Reading, MA, 1981).

[8]F. Butler, in *Lattice '88,* Proceedings of the International Sym-

posium, Batavia, Illinois, 1988, edited by A. S. Kronfeld and P.B. Mackenzie [Nucl. Phys. B (Proc. Suppl.) **9**, 557 (1989)].
[9]S. Duane, A. Kennedy, B. Pendleton, and D. Roweth, Phys. Lett. B **195**, 216 (1987).
[10]K. Binder *et al.*, Phys. Rev. B **34**, 1841 (1986).
[11]H.-Q. Ding, J. Comput. Phys. **67**, 28 (1986).
[12]R. Gavai *et al.*, Phys. Lett. B **241**, 567 (1990).
[13]F. R. Brown *et al.*, Phys. Lett. B **251**, 181 (1990).